


# Formation Dynamics of Potassium-Based Graphite Intercalation Compounds: An *Ab Initio* Study

Xiankai Jiang,<sup>1</sup> Bo Song,<sup>1</sup> and David Tománek<sup>2,\*</sup>

<sup>1</sup>*Terahertz Technology Innovation Research Institute, Shanghai Key Lab of Modern Optical System, Terahertz Science Cooperative Innovation Center, School of Optical-Electrical Computer Engineering, University of Shanghai for Science and Technology, Shanghai 200093, People's Republic of China*

<sup>2</sup>*Physics and Astronomy Department, Michigan State University, East Lansing, Michigan 48824-2320, USA*

 (Received 6 October 2017; revised manuscript received 18 January 2018; published 10 April 2018)

*This paper is a contribution to the Physical Review Applied collection in memory of Mildred S. Dresselhaus.*

We use *ab initio* molecular dynamics simulations to study the microscopic dynamics of potassium intercalation in graphite. Upon adsorbing on graphite from the vapor phase, K atoms transfer their valence charge to the substrate. K atoms adsorbed on the surface diffuse rapidly along the graphene basal plane and eventually enter the interlayer region following a “U-turn” across the edge, gaining additional energy. This process is promoted at higher coverages associated with higher K pressure, leading to the formation of a stable intercalation compound. We find that the functionalization of graphene edges is an essential prerequisite for intercalation since bare edges reconstruct and reconnect, closing off the entry channels for the atoms.

DOI: 10.1103/PhysRevApplied.9.044015

## I. INTRODUCTION

An important aspect of the current research focusing on renewable energy sources is the development of low-cost and large-scale energy storage systems, which are key to the practical use of such energy, which suffers from intermittent energy flow [1]. Some of the most advanced electrochemical energy storage media use graphite intercalation compounds (GICs) [2] as the anode material [3,4]. GIC-based batteries combine a high charge-and-discharge rate with a high energy density, a low weight, and a high number of useful cycles [3,5]. Under optimal conditions, lithium has been shown to intercalate graphite up to the stoichiometric composition of  $\text{LiC}_6$ , yielding a reversible capacity of 372 mA h/g for the graphitic anode [3]. As one of the most efficient energy storage systems, lithium-ion batteries (LIBs) [3–5] have been used extensively for decades now [5–8]. The limited availability and the high cost of lithium [9–11] have been the main reasons driving alternative development of sodium-ion batteries (SIBs) [12–16] and potassium-ion batteries (PIBs) [17–21] using the more abundant and less costly alkali elements Na and K. Microscopic understanding of the kinetics of alkali atoms entering and leaving the region between graphene layers is the key to understanding the rate of charging and discharging, as well as the number of useful cycles, of GIC-based next-generation energy storage systems and devices.

Compared to GIC-based batteries containing Li (LIBs) with a high redox potential of  $-3.04$  V vs the standard hydrogen electrode, the corresponding redox potential of K-based PIBs is only slightly smaller, at  $-2.93$  V, and that of Na-based SIBs is still smaller, with a value of  $-2.71$  V. Since the redox potential is linked to the output voltage and energy density, SIBs do not appear to be very attractive for industrial applications [22–24]. Because of their higher output voltage and energy density, PIBs [25] appear to be a much more attractive low-cost alternative to LIBs. Computational results [26] indicate that K-based GICs are energetically stable up to the high K density in  $\text{KC}_8$ . Recently, potassium GICs were used to develop suitable anode materials for high-performance PIBs [17–19,27–31]. Most of the previous studies have concentrated on the structure and electrochemical performance [32] and have not addressed the microscopic processes occurring in the K-graphite system.

To cover this aspect of the PIB performance, we use *ab initio* canonical molecular dynamics (MD) simulations at high temperatures to obtain microscopic insight into the dynamics of potassium intercalation and diffusion in graphite. The complexity of the potassium intercalation process in the real systems present in batteries is substantial. Scanning-electron-microscopy studies indicate that graphitic crystallites contained in alkali-ion batteries display a large variety of shapes [33]. To further complicate things, the cathode surface is, furthermore, protected by a solid electrolyte interphase (SEI) layer in commercial

\*tomanek@pa.msu.edu

alkali-ion batteries [33]. Variations in the layer stacking, edge morphology, termination, and functionalization are vast, and their consideration exceeds the scope of a single computational study. We address only selected aspects of the intercalation process that occur in a related, simple system, namely, a finite-width graphene bilayer nanoribbon with zigzag edges. This system contains both surface and edge sites and is computationally treatable in MD simulations covering relevant time periods. Our approach provides a realistic representation of the morphology, stability, and interlayer interaction in the graphitic system, the site-specific interaction of K with the graphitic system and its chemically passivated edges, and the dynamically changing interlayer spacing and layer stacking, net charge, and repulsion between K atoms. Most of these aspects have not been addressed in published results of static studies with a constrained geometry [34].

Even though the graphene bilayer ribbon system is very simple, it displays surface diffusion of alkali atoms and their entry into the interlayer space either from free (intergrain) space or by a “U-turn” across the ribbon edge from the surface into the adjacent interlayer region. These three processes are bound to occur also in realistic graphitic grains during intercalation on any alkalis. Therefore, our results are of interest also for related systems, especially in the case of initial low-density intercalation.

We establish the necessity of passivating the flake edges since, otherwise, they may reconnect and close off the entry channels. Our simulations show that potassium can successfully enter the region between the two graphene layers, representing intercalation, and also deintercalate from the flake. The intercalation efficiency can be greatly increased by increasing the K vapor concentration. We find that K atoms gain 0.7 eV when adsorbing on the surface of the graphene bilayer, transferring a large fraction of their valence charge to graphite, then diffuse efficiently along the graphene basal plane forming the surface since the energy barriers for diffusion are very small. Upon reaching the edge, the K atoms perform a U-turn normal to the basal plane and enter the interlayer region. This intercalation process is more probable than the alternative process of free K atoms reaching the edge of the multilayer flake and directly entering the interlayer space.

## II. COMPUTATIONAL TECHNIQUES

Our *ab initio* calculations are based on density-functional theory (DFT), as implemented in the SIESTA package [35]. We use the local-density approximation (LDA) for the exchange-correlation potential [36,37] since it provides a reasonable description of the graphite geometry and elastic properties. We note that in the related layered black phosphorus system, LDA was found to be in much better agreement with results of high-level quantum Monte Carlo calculations than most of the more recently developed exchange-correlation functionals that explicitly

consider van der Waals interactions [38]. A validation of the DFT-LDA approach for graphite was provided previously [39,40], and additional information is contained in the Appendix. We describe valence electrons by norm-conserving Troullier-Martins pseudopotentials [41] and use double- $\zeta$  polarized atomic orbital wave functions [35,42] as a basis. The Fourier expansion of the charge density is truncated at a very high energy cutoff of 350 Ry. The energy shift determining the confinement of atomic orbitals is kept at 0.02 Ry. The small Brillouin zone of the quasi-one-dimensional strips is sampled by a  $1 \times 8 \times 1$   $k$ -point grid [43]. All of the static geometries are optimized using the conjugate gradient method [44] until none of the residual Hellmann-Feynman forces acting on any atom exceed  $0.05 \text{ eV}/\text{\AA}$ . Extensive canonical MD calculations are performed at constant volume using a Nosé thermostat at  $T = 900 \text{ K}$  for time periods up to 4.5 ps, using time steps of 0.3 fs. While this approach requires extensive computer resources and limits the number of trajectories, the results for systems with large dynamical charge redistribution are expected to be more reliable than alternative treatments using parametrized force fields.

## III. RESULTS

The graphene bilayer system we consider is represented by a periodic array of infinite strips with hydrogen-terminated zigzag edges, as seen in Figs. 1(a) and 1(b). The initial configuration consists of two AA-stacked graphene ribbons with a width of  $15.74 \text{ \AA}$  and an interlayer separation of  $3.34 \text{ \AA}$ . The strips lie in the  $x$ - $y$  plane, with the  $y$  axis forming the strip center. The orthorhombic unit cell is  $21.00 \text{ \AA}$  wide,  $9.89 \text{ \AA}$  long, and  $10.00 \text{ \AA}$  high, and it contains 128 carbon atoms in total. These cell dimensions

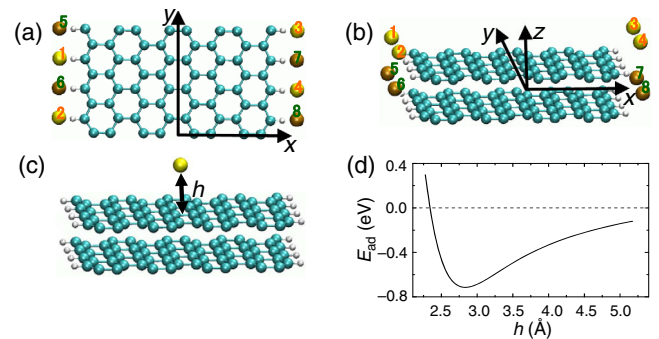
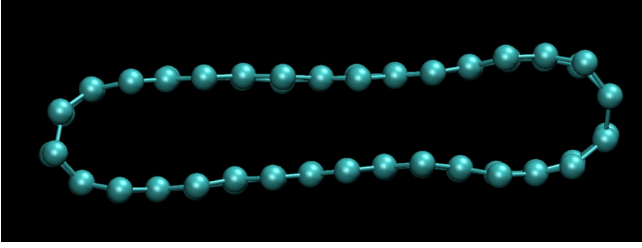


FIG. 1. Initial geometry of the AA-stacked graphene bilayer  $C_{128}H_{16}$  unit cell with eight K atoms in the molecular dynamics simulations, presented in (a) a top and (b) a perspective view. Potassium atoms are represented by the labeled large yellow balls, hydrogen atoms by small white balls, and carbon atoms by cyan balls. Of the eight K atoms per unit cell, four—shown in light yellow—are above the surface and the other four—shown in dark yellow—are near the interlayer region. (c) The geometry and (d) the binding energy of a K atom interacting with the graphene bilayer surface.



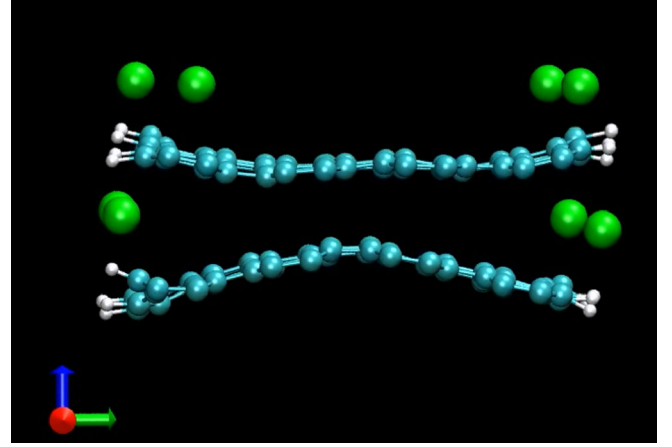
**VIDEO 1.** Spontaneous reconstruction and reconnection of unpassivated edges of a finite-width graphene bilayer in an end-on view.

decouple the bilayer strips in the periodic arrangement and provide sufficient space for the hydrogen termination and eight free potassium atoms. The eight potassium atoms are distributed uniformly in the vacuum area, with the initial coordinates (in angstrom units)  $\mathbf{r}_1 = (-9.87, 0.00, 1.67)$ ,  $\mathbf{r}_2 = (-9.87, -4.97, 1.67)$ ,  $\mathbf{r}_3 = (9.87, -2.49, 5.34)$ ,  $\mathbf{r}_4 = (9.87, -7.46, 5.34)$ ,  $\mathbf{r}_5 = (-9.87, -2.49, 1.67)$ ,  $\mathbf{r}_6 = (-9.87, -7.46, 1.67)$ ,  $\mathbf{r}_7 = (9.87, 0.00, 5.34)$ , and  $\mathbf{r}_8 = (9.87, -4.97, 5.34)$ , as shown in Fig. 1. The unit cell is charge neutral throughout the work.

To calibrate our simulation conditions, we first perform MD simulations of the graphene bilayer strip using graphene nanoribbons with bare edges. We find that the edges reconnect spontaneously on a time scale of 1 ps, thus blocking off the entry channels into the interlayer region, as seen in Video 1. We conclude that passivation of the exposed edges is a necessary prerequisite for achieving intercalation. Therefore, we saturate all exposed graphene edges with hydrogen in all of our following work.

Because of the considerable computer resources required to run extended MD simulations, we can only perform a limited number of runs, which is insufficient to obtain reliable ensemble averages. Clearly, individual molecular dynamics trajectories, which we discuss below, have only limited statistical value. Nevertheless, we believe that they provide a valuable illustration of the kinetics of the graphite intercalation process.

Placing K atoms in the positions stated above, we perform several MD runs with 15 000 time steps each, spanning 4.5 ps in total. We find that the K atoms adsorb at  $h = 2.8 \text{ \AA}$ , gaining 0.7 eV, as seen in Figs. 1(c) and 1(d). Our Mulliken population analysis [45] indicates that the K atoms transfer between 0.4 and 0.5 electrons to the graphitic system as they adsorb on top or enter the interlayer region of the bilayer, so they should be viewed as K atoms. We observe that the K atoms, labeled 1–4 in Fig. 1, first diffuse rapidly along the graphite surface due to very low diffusion barriers [46] of  $\lesssim 0.1 \text{ eV}$ . Concurrently, K atoms labeled 5–8 penetrate into the interlayer space, representing intercalation, and occasionally also leave this space, representing deintercalation. This process is depicted in Video 2. In order to describe the dynamical process of K intercalation and deintercalation



**VIDEO 2.** Diffusion and intercalation of K atoms on a finite-width graphene bilayer with H-passivated edges in an end-on view.

quantitatively, we monitor at each time step the distance  $d_i(t)$  between each K atom  $i$  and the nearest graphitic edge, defined by

$$d_i(t) = \text{sgn}(x_i(t))x_i(t) - \langle x_e \rangle(t). \quad (1)$$

Here,  $x_i$  is the  $x$  coordinate of atom  $i$  and  $\langle x_e \rangle$  is the average  $x$  coordinate of the atoms forming the right edge of the strip, with  $\langle x_e \rangle > 0$ , according to the geometry shown in Fig. 2(a). Definition (1) makes sense for our purpose since we mainly want to distinguish whether a K atom is inside our outside the strip and we do not care or if it is closer to

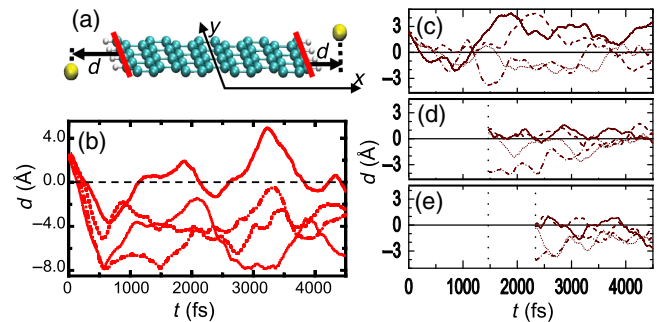


**FIG. 2.** Diffusion behavior of K atoms interacting with a graphene bilayer. (a) Perspective view of the K-graphite system, with  $d$  defining the horizontal distance outside the closest of the two edges, highlighted by the solid red lines. (b) Diffusion characteristic of the four K atoms, labeled 1–4 in Figs. 1(a) and 1(b), which are initially placed above the strip. (c) Diffusion characteristic of the other four K atoms, labeled 5–8 in Figs. 1(a) and 1(b), which are initially placed near the interlayer region. (d) Change in the diffusion characteristics of atoms in (c) induced by an increase of K vapor pressure at  $t = 1470 \text{ fs}$ , modeled by placing four additional alkali atoms near the interlayer region. (e) Change in the diffusion characteristics of atoms in (d) induced by a further increase of K vapor pressure at  $t = 2340 \text{ fs}$ , modeled by placing two additional alkali atoms near the interlayer region.



the left or to the right edge. According to the definition,  $d > 0$  indicates “outside” and  $d < 0$  indicates “inside” the strip, either near the surface or between the layers.

According to the initial conditions defined above, the K atoms labeled 1, 2, 5, and 6 are initially placed 2 Å outside the left edge, and the atoms labeled 3, 4, 7, and 8 are initially placed 2 Å outside the right edge, with  $d_i(t=0) = +2$  Å for  $i = 1, \dots, 8$  as seen in Figs. 2(b) and 2(c). The trajectories  $d(t)$  in these subfigures indicate a rapid diffusion of the atoms.

In the following, we discuss the atomic motion displayed in Figs. 2(b) and 2(c) in more detail from the viewpoint of intercalation and deintercalation. As seen in Fig. 2(b), atoms initially placed above the strip approach the nearest edge during about the first 220 fs. The trajectory of the K atom labeled 1 in Fig. 1 is shown by the solid line in Fig. 2(b). As a function of time, this atom spends consecutive time periods of approximately 1 ps alternatively inside or outside the bilayer, relatively close to the edge, indicating efficient intercalation and deintercalation. The remaining three K atoms, labeled 2–4, intercalate into the interlayer region and never exit it, according to Fig. 2(b). Depending on the K concentration in the interlayer region, we find the interlayer distance to increase by an amount  $\lesssim 70\%$ .

Somewhat similar behavior is observed in Fig. 2(c) for the K ions labeled 5–8 in Fig. 1, which had originally been placed not above the strip but near the interlayer region. After reaching the strip edge during about the first 200 fs, two of the atoms enter into the interlayer region and two remain outside, never farther than approximately 3 Å from the nearest edge.

To study the effect of potassium vapor pressure on the intercalation process, we stop the MD simulation after  $t = 1470$  fs and introduce four additional alkali atoms near the interlayer region. The dynamics of the K atoms in the unit cell that now contain two  $C_{64}H_8$  nanoribbon segments and 12 K atoms is shown in Fig. 2(d). With increasing time, we find that most of the atoms remain outside, close to the edge, or approach the edge from the inside region.

At  $t = 2340$  fs, we stop the MD simulation again, as illustrated in Fig. 2(d), and introduce two additional K atoms into the unit cell. The dynamics of the system that now contain 14 K atoms in the unit cell is shown in Fig. 2(e). Compared to the results in Figs. 2(c) and 2(d) at lower pressures of K, we observe that most K atoms penetrate into the interlayer region and remain there over time, driven by the gain in chemical potential. These results clearly indicate the benefit of a high K concentration outside the graphite flakes on K atom intercalation.

During our simulations, we observe one K atom, adsorbed on top of the graphitic surface, to perform a U-turn across the edge into the region between the graphene layers. This process is visualized in Fig. 3 and Video 3. Figure 3(a) defines the dihedral angle  $\alpha$  between

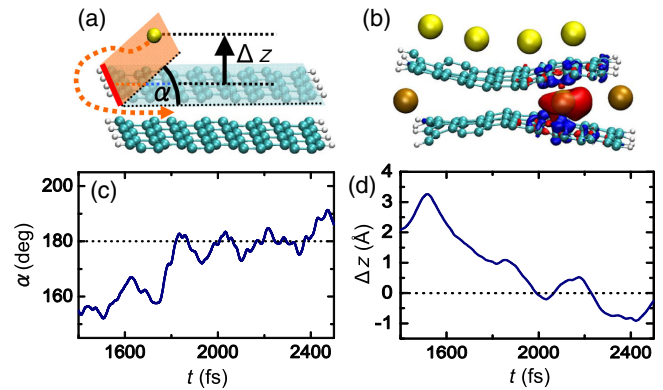
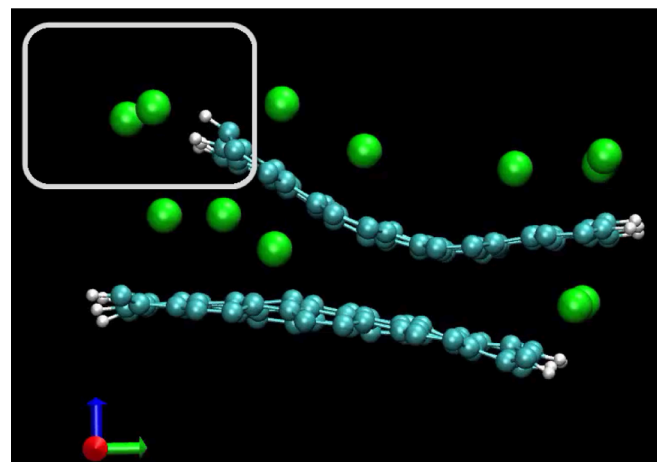


FIG. 3. Microscopic kinetics of K intercalation in graphite. (a) Geometry of the U-turn process. The horizontal graphene plane is shown in light blue, with its edge enhanced by the red line. Another plane, shown in orange, contains a K atom, and the graphene edge is shown in red. The dihedral angle  $\alpha$  is the angle between these planes.  $\Delta z$  is the distance between the K atom and the graphene layer. (b) Snapshot of atomic positions at  $t = 1470$  fs during the intercalation process, superposed with a representation of the charge flow due to the insertion of a K atom into the interlayer region. The entry of K increases the interlayer distance by  $\lesssim 70\%$ . The charge density difference  $\Delta\rho = \rho_{\text{tot}}(C_{128}H_{16} + 8 \text{ K}) - \rho_{\text{tot}}(\text{K}) - \rho_{\text{tot}}(C_{128}H_{16} + 7 \text{ K})$  is presented by the isosurfaces of the excess negative charge at  $\Delta\rho = +10^{-3} e/\text{\AA}^3$ , shown in blue, and the negative charge deficit at  $\Delta\rho = -10^{-3} e/\text{\AA}^3$ , shown in red. The potassium atom in the center of the red cloud loses 0.531 electrons. (c) Time dependence of the dihedral angle  $\alpha$  during the U-turn of a K atom from the surface region, across the edge, to the area between the graphene layers. (d) Time dependence of the vertical position  $\Delta z$  of a K atom during the intercalation process.  $\alpha < 180^\circ$  and  $\Delta z > 0$  indicate that the K atom is above the graphitic surface.  $\alpha > 180^\circ$  and  $\Delta z < 0$  indicate that the K atom is between the graphene layers.



VIDEO 3. Intercalation of a K atom by performing a U-turn from the region above the bilayer, across the edge, to the region between the layers in an end-on view. The region of interest is highlighted by the white frame.

the plane containing this K atom and the closest edge of a graphene ribbon and the surface of this graphene ribbon, as well as the height  $\Delta z$  of the atom above the top graphene layer. The charge-density difference  $\Delta\rho$ , superposed to the atomic structure in Fig. 3(b), indicates an opening of the interlayer distance at the point of K entry and charge flow from the K site to the neighboring graphitic layers. As seen in Fig. 3(c), the dihedral angle associated with this K atom lies below  $180^\circ$  for  $t \lesssim 1820$  fs, indicating that the K atom is initially on top of the graphitic surface. For  $t \gtrsim 2370$  fs, the dihedral angle exceeds  $180^\circ$ , meaning that the K atom has entered the interlayer region. This conclusion is consistent with the plot of the atom's vertical position  $\Delta z$  above the topmost layer in Fig. 3(d).

#### IV. SUMMARY AND CONCLUSIONS

In summary, we investigate in this paper the intercalation of potassium into a graphene bilayer at  $T = 900$  K by *ab initio* DFT molecular dynamics simulations. We find that an essential prerequisite for alkali intercalation is the passivation of graphitic edges, which otherwise reconstruct and reconnect, closing up the entry channels for the alkali atoms. Our simulations indicate that potassium atoms can easily intercalate and deintercalate the graphene bilayer with passivated edges. Increasing the K vapor concentration promotes the intercalation. We observe that K atoms gain energy by adsorbing on the graphene bilayer and may diffuse efficiently along its surface after losing 0.4–0.5 electrons to the graphitic system. Upon reaching the edge, K atoms may undergo a U-turn across the edge and enter the interlayer region. Depending on the K concentration in the interlayer region, we find the graphite interlayer distance to increase by an amount  $\lesssim 70\%$ .

Of course, our computational results—however demanding on computer resources—cover only specific aspects of the alkali intercalation process in graphite. Even though several MD runs are performed for unusually long run times of 4.5 ps and the system is believed to be ergodic, the information is insufficient for providing valid ensemble averages. A graphene bilayer nanoribbon of finite width may provide a semiquantitative representation at best of the intercalation process occurring in a realistic graphite flake. The heat-bath temperature of 900 K, used in our work as a common way to accelerate the dynamics of the MD simulation, is much higher than the temperatures used in the experiment.

Clearly, for realistic future studies of alkali-ion batteries, much attention has to be paid to the morphology and chemical functionalization of the graphite edges. Important insight can be obtained from static structure optimization calculations of the type reported in Ref. [34]. As our work indicates, however, it is essential not to constrain the unit-cell geometry so that the interlayer separation may change, and to consider the Coulomb repulsion between charged alkali atoms. Of great interest for future calculations are

also observations of the average shape of graphite grains present in alkali-ion batteries, which should determine the relative importance of the basal planes at the surface. We believe that the results of our microscopic molecular dynamics simulations provide specific insight that should be helpful for the development and optimization of GIC-based energy storage systems and devices.

#### ACKNOWLEDGMENTS

D. T. acknowledges the financial support from National Science Foundation - Air Force Office of Scientific Research (NSF-AFOSR) EFRI 2-DARE Grant No. EFMA-1433459.

#### APPENDIX: VALIDATION OF THE LDA EXCHANGE-CORRELATION FUNCTIONAL IN GRAPHITE AND RELATED SYSTEMS

There is significant interest in determining theoretically the equilibrium geometry and interlayer binding energy in layered, so-called van der Waals materials such as graphite, where the interlayer interaction is significantly affected by the dispersive van der Waals interaction. From the viewpoint of precision, quantum Monte Carlo (QMC) calculations are believed to give the most reliable results and have been applied to graphite [47] and related layered bulk black phosphorus [38]. Since the computational cost makes QMC calculations impracticably expensive, the method of choice is DFT with various approximations for the exchange-correlation (XC) functional. Historically, the LDA has been used first [36,37], but it is believed to underestimate the van der Waals interaction. Many XC functionals have been developed since, and their predictions for bulk and bilayer black phosphorus are compared in Ref. [38]. The results are stunning: depending on the XC functional, the interlayer binding may change by a factor of up to 10. It is very interesting to note that, among these results, LDA predictions are consistently closest to the most dependable QMC results.

DFT-LDA calculations for graphite were validated by selected experimental results in Ref. [48]. The calculated equilibrium in-plane lattice constant value  $a_0 = 2.451$  Å is in excellent agreement with the observed value  $a_0 = 2.456$  Å reported in Ref. [49]. The calculated interlayer distance  $d = 3.36$  Å is in equally good agreement with the observed value  $d = 3.34$  Å reported in Ref. [50]. The calculated interplanar binding energy  $E_b = 25$  meV/atom is in very good agreement with the observed value  $E_b = 22.8$  meV/atom reported in Ref. [40]. DFT-LDA results for the elastic response of graphite are in excellent agreement with the Raman measurements of multilayer graphene reported in Ref. [51].

The LDA value of the equilibrium distance  $d_a = 2.77$  Å between K and the surface of graphite, reported in Ref. [52], is in excellent agreement with the LEED value  $d_a = 2.79 \pm 0.03$  Å of Ref. [53]. The charge transfer

between K and graphite predicted by LDA agrees very well with the Raman data of Ref. [54]. Thus, the DFT LDA is believed to provide a dependable description of graphite and K-based graphite intercalation compounds.

- 
- [1] Kaixiang Lin, Qing Chen, Michael R. Gerhardt, Liuchuan Tong, Sang Bok Kim, Louise Eisenach, Alvaro W. Valle, David Hardee, Roy G. Gordon, Michael J. Aziz, and Michael P. Marshak, Alkaline quinone flow battery, *Science* **349**, 1529 (2015).
- [2] M. S. Dresselhaus and G. Dresselhaus, Intercalation compounds of graphite, *Adv. Phys.* **51**, 1 (2002).
- [3] M. Endo, C. Kim, K. Nishimura, T. Fujino, and K. Miyashita, Recent development of carbon materials for Li ion batteries, *Carbon* **38**, 183 (2000).
- [4] Y. Nishi, Lithium ion secondary batteries: past 10 years and the future, *J. Power Sources* **100**, 101 (2001).
- [5] A. S. Aricò, P. Bruce, B. Scrosati, J.-M. Tarascon, and W. van Schalkwijk, Nanostructured materials for advanced energy conversion and storage devices, *Nat. Mater.* **4**, 366 (2005).
- [6] Bruce Dunn, Haresh Kamath, and Jean-Marie Tarascon, Electrical energy storage for the grid: A battery of choices, *Science* **334**, 928 (2011).
- [7] S. Chu and A. Majumdar, Opportunities and challenges for a sustainable energy future, *Nature (London)* **488**, 294 (2012).
- [8] M. Armand and J.-M. Tarascon, Building better batteries, *Nature (London)* **451**, 652 (2008).
- [9] L. Fan, R. Ma, Y. Yang, S. Chen, and B. Lu, Covalent sulfur for advanced room temperature sodium-sulfur batteries, *Nano Energy* **28**, 304 (2016).
- [10] Y. X. Wang, J. Yang, S. L. Chou, H. K. Liu, W. Zhang, D. Zhao, and S. X. Dou, Uniform yolk-shell iron sulfide-carbon nanospheres for superior sodium-iron sulfide batteries, *Nat. Commun.* **6**, 8689 (2015).
- [11] J. Sun, H.-W. Lee, M. Pasta, H. Yuan, G. Zheng, Y. Sun, Y. Li, and Y. Cui, A phosphorene-graphene hybrid material as a high-capacity anode for sodium-ion batteries, *Nat. Nanotechnol.* **10**, 980 (2015).
- [12] N. Yabuuchi, K. Kubota, M. Dahbi, and S. Komaba, Research development on sodium ion batteries, *Chem. Rev.* **114**, 11636 (2014).
- [13] Sung-Wook Kim, Dong-Hwa Seo, Xiaohua Ma, Gerbrand Ceder, and Kisuk Kang, Electrode materials for rechargeable sodium-ion batteries: Potential alternatives to current lithium-ion batteries, *Adv. Energy Mater.* **2**, 710 (2012).
- [14] Xingde Xiang, Kai Zhang, and Jun Chen, Recent advances and prospects of cathode materials for sodium-ion batteries, *Adv. Mater.* **27**, 5343 (2015).
- [15] Verónica Palomares, Paula Serras, Irune Villaluenga, Karina B. Hueso, Javier Carretero-González, and Teófilo Rojo, Na-ion batteries, recent advances and present challenges to become low cost energy storage systems, *Energy Environ. Sci.* **5**, 5884 (2012).
- [16] Huilin Pan, Yong-Sheng Hu, and Liquan Chen, Room-temperature stationary sodium-ion batteries for large-scale electric energy storage, *Energy Environ. Sci.* **6**, 2338 (2013).
- [17] Zelang Jian, Wei Luo, and Xiulei Ji, Carbon electrodes for K-ion batteries, *J. Am. Chem. Soc.* **137**, 11566 (2015).
- [18] Wei Luo, Jiayu Wan, Burak Ozdemir, Wenzhong Bao, Yanan Chen, Jiaqi Dai, Hao Lin, Yue Xu, Feng Gu, Veronica Barone, and Liangbing Hu, Potassium ion batteries with graphitic materials, *Nano Lett.* **15**, 7671 (2015).
- [19] Shinichi Komaba, Tatsuya Hasegawa, Mouad Dahbi, and Kei Kubota, Potassium intercalation into graphite to realize high-voltage/high-power potassium-ion batteries and potassium-ion capacitors, *Electrochem. Commun.* **60**, 172 (2015).
- [20] Ying Liu, Feifei Fan, Jiangwei Wang, Yang Liu, Hailong Chen, Katherine L. Jungjohann, Yunhua Xu, Yujie Zhu, David Bigio, Ting Zhu, and Chunsheng Wang, *In situ* transmission electron microscopy study of electrochemical sodiation and potassiation of carbon nanofibers, *Nano Lett.* **14**, 3445 (2014).
- [21] R. Tossici, M. Berrettoni, M. Rosolen, R. Marassi, and B. Scrosati, Electrochemistry of KC<sub>8</sub> in lithium-containing electrolytes and its use in lithium-ion cells, *J. Electrochem. Soc.* **144**, 186 (1997).
- [22] Dipan Kundu, Elahe Talaie, Victor Duffort, and Linda F. Nazar, The emerging chemistry of sodium ion batteries for electrochemical energy storage, *Angew. Chem., Int. Ed. Engl.* **54**, 3431 (2015).
- [23] Verónica Palomares, Montse Casas-Cabanas, Elizabeth Castillo-Martínez, Man H. Han, and Teófilo Rojo, Update on Na-based battery materials. A growing research path, *Energy Environ. Sci.* **6**, 2312 (2013).
- [24] Sung You Hong, Youngjin Kim, Yuwon Park, Aram Choi, Nam-Soon Choi, and Kyu Tae Lee, Charge carriers in rechargeable batteries: Na ions vs. Li ions, *Energy Environ. Sci.* **6**, 2067 (2013).
- [25] Wenchao Zhang, Jianfeng Mao, Sean Li, Zhixin Chen, and Zaiping Guo, Phosphorus-based alloy materials for advanced potassium-ion battery anode, *J. Am. Chem. Soc.* **139**, 3316 (2017).
- [26] K. Nobuhara, H. Nakayama, M. Nose, S. Nakanishi, and H. Iba, First-principles study of alkali metal-graphite intercalation compounds, *J. Power Sources* **243**, 585 (2013).
- [27] K. Beltrop, S. Beuker, A. Heckmann, M. Winter, and T. Placke, Alternative electrochemical energy storage: Potassium-based dual-graphite batteries, *Energy Environ. Sci.* **10**, 2090 (2017).
- [28] Ling Fan, Qian Liu, Suhua Chen, Kairui Lin, Zhi Xu, and Bingan Lu, Potassium-based dual ion battery with dual-graphite electrode, *Small* **13**, 1701011 (2017).
- [29] K. Share, A. P. Cohn, R. Carter, B. Rogers, and C. L. Pint, Role of nitrogen-doped graphene for improved high-capacity potassium ion battery anodes, *ACS Nano* **10**, 9738 (2016).
- [30] Z. Ju, S. Zhang, Z. Xing, Q. C. Zhuang, Y. H. Qiang, and Y. Qian, Direct synthesis few-layer F-doped graphene foam and its lithium/potassium storage properties, *ACS Appl. Mater. Interfaces* **8**, 20682 (2016).
- [31] K. Share, A. P. Cohn, R. E. Carter, and C. L. Pint, Mechanism of potassium ion intercalation staging in few layered graphene from *in situ* Raman spectroscopy, *Nanoscale* **8**, 16435 (2016).



- [32] Jin Zhao, Xiaoxi Zou, Yujie Zhu, Yunhua Xu, and Chunsheng Wang, Electrochemical intercalation of potassium into graphite, *Adv. Funct. Mater.* **26**, 8103 (2016).
- [33] P. Verma, P. Maire, and P. Novák, A review of the features and analyses of the solid electrolyte interphase in Li-ion batteries, *Electrochim. Acta* **55**, 6332 (2010).
- [34] Takazumi Kawai, First principles calculations for diffusion barriers of lithium intercalation into graphite with various edge terminations, *Jpn. J. Appl. Phys.* **52**, 04CN08 (2013).
- [35] José M. Soler, Emilio Artacho, Julian D. Gale, Alberto García, Javier Junquera, Pablo Ordejón, and Daniel Sánchez-Portal, The SIESTA method for *ab initio* order- $N$  materials simulation, *J. Phys. Condens. Matter* **14**, 2745 (2002).
- [36] D.M. Ceperley and B.J. Alder, Ground State of the Electron Gas by a Stochastic Method, *Phys. Rev. Lett.* **45**, 566 (1980).
- [37] J.P. Perdew and A. Zunger, Self-interaction correction to density-functional approximations for many-electron systems, *Phys. Rev. B* **23**, 5048 (1981).
- [38] Luke Shulenberger, Andrew D. Baczewski, Zhen Zhu, Jie Guan, and David Tomanek, The nature of the interlayer interaction in bulk and few-layer phosphorus, *Nano Lett.* **15**, 8170 (2015).
- [39] Matthias C. Schabel and José Luís Martins, Energetics of interplanar binding in graphite, *Phys. Rev. B* **46**, 7185 (1992).
- [40] L. A. Girifalco and R. A. Lad, Energy of cohesion, compressibility, and the potential energy functions of the graphite system, *J. Chem. Phys.* **25**, 693 (1956).
- [41] N. Troullier and J.L. Martins, Efficient pseudopotentials for plane-wave calculations, *Phys. Rev. B* **43**, 1993 (1991).
- [42] D. Sánchez-Portal, P. Ordejón, E. Artacho, and J. M. Soler, Density-functional method for very large systems with LCAO basis sets, *Int. J. Quantum Chem.* **65**, 453 (1997).
- [43] Hendrik J. Monkhorst and James D. Pack, Special points for Brillouin-zone integrations, *Phys. Rev. B* **13**, 5188 (1976).
- [44] M.R. Hestenes and E. Stiefel, Methods of conjugate gradients for solving linear systems, *J. Res. Natl. Bur. Stand.* **49**, 409 (1952).
- [45] R.S. Mulliken, Electronic population analysis on LCAO-MO molecular wave functions. I, *J. Chem. Phys.* **23**, 1833 (1955).
- [46] Kevin T. Chan, J. B. Neaton, and Marvin L. Cohen, First-principles study of metal adatom adsorption on graphene, *Phys. Rev. B* **77**, 235430 (2008).
- [47] Leonardo Spanu, Sandro Sorella, and Giulia Galli, Nature and Strength of Interlayer Binding in Graphite, *Phys. Rev. Lett.* **103**, 196401 (2009).
- [48] M. C. Schabel and J. L. Martins, Energetics of interplanar binding in graphite, *Phys. Rev. B* **46**, 7185 (1992).
- [49] Y. Baskin and L. Meyer, Lattice constants of graphite at low temperatures, *Phys. Rev.* **100**, 544 (1955).
- [50] R. Nicklow, N. Wakabayashi, and H.G. Smith, Lattice dynamics of pyrolytic graphite, *Phys. Rev. B* **5**, 4951 (1972).
- [51] P.H. Tan, W.P. Han, W.J. Zhao, Z.H. Wu, K. Chang, H. Wang, Y.F. Wang, N. Bonini, N. Marzari, N. Pugno, G. Savini, A. Lombardo, and A. C. Ferrari, The shear mode of multilayer graphene, *Nat. Mater.* **11**, 294 (2012).
- [52] F. Ancilotto and F. Toigo, First-principles study of potassium adsorption on graphite, *Phys. Rev. B* **47**, 13713 (1993).
- [53] N. Ferralis, K. Pussi, S.E. Finberg, J. Smerdon, M. Lindroos, R. McGrath, and R. D. Diehl, Low-energy electron diffraction study of potassium adsorbed on single-crystal graphite and highly oriented pyrolytic graphite, *Phys. Rev. B* **70**, 245407 (2004).
- [54] J. C. Chacón-Torres, L. Wirtz, and T. Pichler, Manifestation of charged and strained graphene layers in the Raman response of graphite intercalation compounds, *ACS Nano* **7**, 9249 (2013).